Quantum Tunneling Enabled Self-Assembly of Hydrogen Atoms on Cu(111)

April D. Jewell,[†] Guowen Peng,[‡] Michael F. G. Mattera,[†] Emily A. Lewis,[†] Colin J. Murphy,[†] Georgios Kyriakou,[†,§] Manos Mavrikakis,[‡] and E. Charles H. Sykes[†,*]

[†]Chemistry Department, Tufts University, 62 Talbot Avenue, Medford, Massachusetts 02155, United States and [‡]Department of Chemical and Biological Engineering, University of Wisconsin-Madison, 1415 Engineering Drive, Madison, Wisconsin 53706, United States . [§]Present address: Department of Chemistry, University of Hull, Cottingham Road, Hull, HU6 7RX, UK.

ABSTRACT

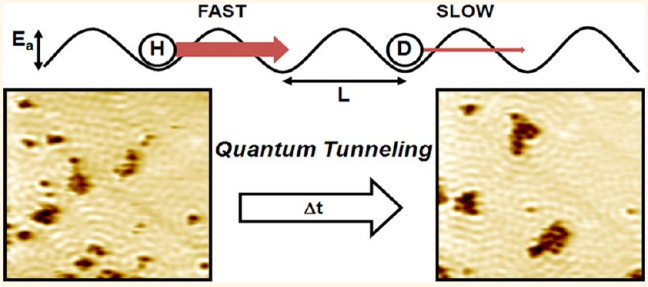

Atomic and molecular self-assembly are key phenomena that underpin many important technologies. Typically, thermally enabled diffusion allows a system to sample many areas of configurational space, and ordered assemblies evolve that optimize interactions between species. Herein we describe a system in which the diffusion is quantum tunneling in nature and report the self-assembly of H atoms on a Cu(111) surface into complex arrays based on local clustering followed by larger scale islanding of these clusters. By scanning tunneling microscope tip-induced scrambling of H atom assemblies, we are able to watch the atomic scale details of H atom self-assembly in real time. The ordered arrangements we observe are complex and very different from those formed by H on other metals that occur in much simpler geometries. We contrast the diffusion and assembly of H with D, which has a much slower tunneling rate and is not able to form the large islands observed with H over equivalent time scales. Using density functional theory, we examine the interaction of H atoms on Cu(111) by calculating the differential binding energy as a function of H coverage. At the temperature of the experiments (5 K), H(D) diffusion by quantum tunneling dominates. The quantum-tunneling-enabled H and D diffusion is studied using a semiclassically corrected transition state theory coupled with density functional theory. This system constitutes the first example of quantum-tunneling-enabled self-assembly, while simultaneously demonstrating the complex ordering of H on Cu(111), a catalytically relevant surface.

KEYWORDS: hydrogen · quantum tunneling · diffusion · self-assembly · STM · Cu(111)

During the past several decades, the self-assembly of chemical species on metal and semiconductor surfaces has been a topic of great interest to the scientific community. Self-assembled monolayers (SAMs) offer a relatively straightforward route for surface modification and tailored chemical functionality, and SAMs have widespread applications in a variety of areas from electronics to biosensing. The organization of atoms and molecules adsorbed on a surface is dependent on a variety of factors pertaining to interactions with the surface and between the adsorbates themselves;[1−4] some aspects to consider include the adsorbate−substrate binding energy, substrate-mediated and direct lateral adsorbate−adsorbate interactions, and charge transfer between adsorbates and the surface. Surface diffusion, or thermal mobility, is also a key driving force in SAM formation, and knowledge of how adsorbates move on a surface is a topic of great importance. For instance, thiol SAMs on Au are by far the most widely studied system in molecular assembly.[5−8] Overlayers are often formed in solution at room temperature, resulting in structures with relatively small domain sizes and high defect densities.[5] These defects result in facile degradation of the SAM; however, it was shown that thermal annealing treatments lead to domain fusion and defect "healing",[9,10] which is a direct effect of an increased rate of lateral diffusion on the surface and improves SAM stability. On a related note, Ertl and co-workers examined the behavior of O on Pt using scanning tunneling microscopy (STM).[11] They showed that at low coverage and 160 K, chemisorbed O atoms exist as randomly distributed pairs; however, at lower temperatures (<140 K) the O pairs form clusters and interconnected, one-dimensional chains on the surface. These observations elucidated the role of already chemisorbed O as the active site for the dissociation of O_2: the O_2 molecules adsorb in a mobile precursor state, diffuse to the active site where O−O bond splitting occurs, and become frozen in place as the chemisorbed O species.[11] Thus, thermally activated adsorbate diffusion can play an important role

* Address correspondence to charles.sykes@tufts.edu.

Received for review August 22, 2012 and accepted October 2, 2012.

Published online October 02, 2012
10.1021/nn3038463

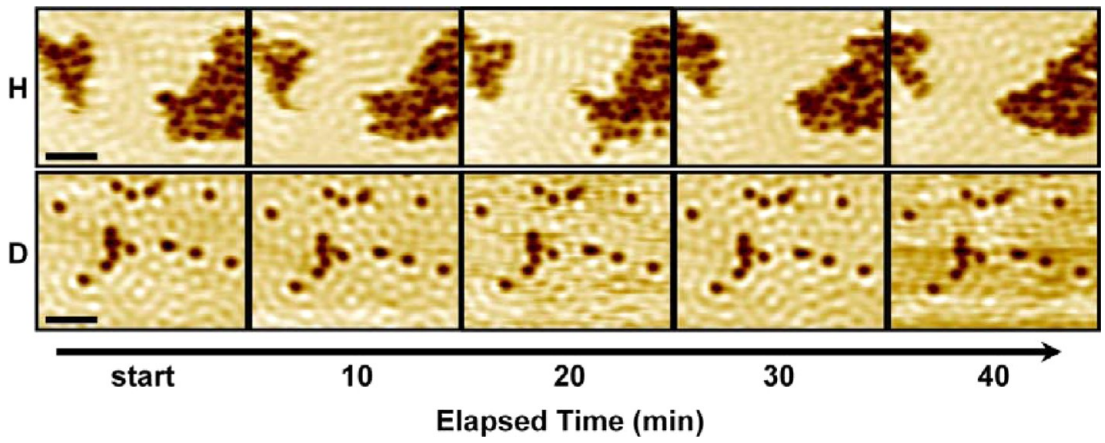

Figure 1. Time-lapse STM images of H (top) and D (bottom) on Cu(111) at 5 K. Time between images is 10 min. Scale bars = 5 nm.

in our understanding of both self-assembled and catalytic systems.

The quantum-tunneling-enabled diffusion of adsorbates was previously observed on a variety of surfaces by field emission microscopy,[12−16] optical diffraction,[17−20] and STM.[21−23] Typically, scanning probe investigations of diffusing species have focused on individual, isolated atoms and molecules;[21−26] however, the interaction and self-assembly of atoms are also of great interest. In this manuscript, we report an experimental and theoretical study of the self-assembly of H atoms into complex and dynamic arrangements on a Cu(111) surface. The use of Pd/Cu single atom alloys allows us to uptake a significant amount of H(D) onto a Cu surface, as compared to the single H(D) atom studies performed by Ho and co-workers.[21] Combining low-temperature STM with density functional theory (DFT) calculations, we find further support for the quantum tunneling diffusion of H(D) adatoms. We discuss the influence of short- and long-range interactions that lead to complex assemblies of H(D) atoms. We show that the short-range interactions result in a stabilization of dimers on the 0.3 nm scale; this phenomenon is especially apparent in the case of D. The tunneling rate of H is orders of magnitude faster than D, allowing H to form large islands due to a weaker long-range interaction between small clusters, which, as we show in the case of D, are dominantly dimers. The experiments described herein were performed at 5 K, well below the temperature regime for activated diffusion, and all of the diffusion and self-assembly observed is quantum tunneling enabled. Differences in rates of motion of H(D) monomers can be explained, not in terms of the barrier height (i.e., as in classical, thermal diffusion), but in terms of tunneling probability, which depends on the barrier height and width, as well as particle mass. Also, the relative energies of the initial and final state levels have an important effect on the tunneling efficiency.[22,27−29]

RESULTS AND DISCUSSION

The dissociative adsorption of H_2 on Cu(111) is known to be an activated process, with a barrier on the order of 400 meV;[30] however, we have recently shown that this barrier can be reduced by adding isolated Pd atoms to the top layer of the Cu(111) metal surface.[31,32] Using this alloy system with a Pd coverage of 0.01 monolayers (ML), we populated a Cu surface with H(D) adatoms, as shown in Figure 1. All data were recorded on Cu(111) terraces far (>20 nm) from the alloyed regions of the surface and as such represent clean Cu(111) as evidenced by the electron standing waves visible in most images. H(D) atoms appear in STM images as shallow depressions (∼10 pm) on the Cu surface due to the lower electron tunneling probability through the H(D) atom-metal complex as compared to the bare metal at energies close to the Fermi level (typically <100 meV).[21,33]

Low-temperature STM imaging offers an advantage in that processes that are normally quite rapid at room temperature are significantly slowed; thus, at 5 K we are able to follow adsorbate diffusion by repeated imaging of the same area. The time-lapse sequence of images in Figure 1 depict the result of adatom diffusion for H (top row) and D (bottom row). These images were taken from STM movies recorded over several hours of continuous scanning. Each image took ∼1 min to acquire; the H and D systems are shown at 10 min intervals. To minimize perturbation by the STM tip we qualitatively examined surface diffusion as a function of tunneling current and found no discernible difference for the diffusion rate of H atoms in the 20−50 pA current range. At tunneling currents >70 pA we noted an increase in the diffusion rate. Therefore, all diffusion rate measurements were performed at 50 pA and 30 mV. These gap conditions are in line with the nonperturbative tunneling conditions used by Wilson Ho and co-workers in their study of H and D on Cu(100).[21] The H(D) diffusion STM movies are available

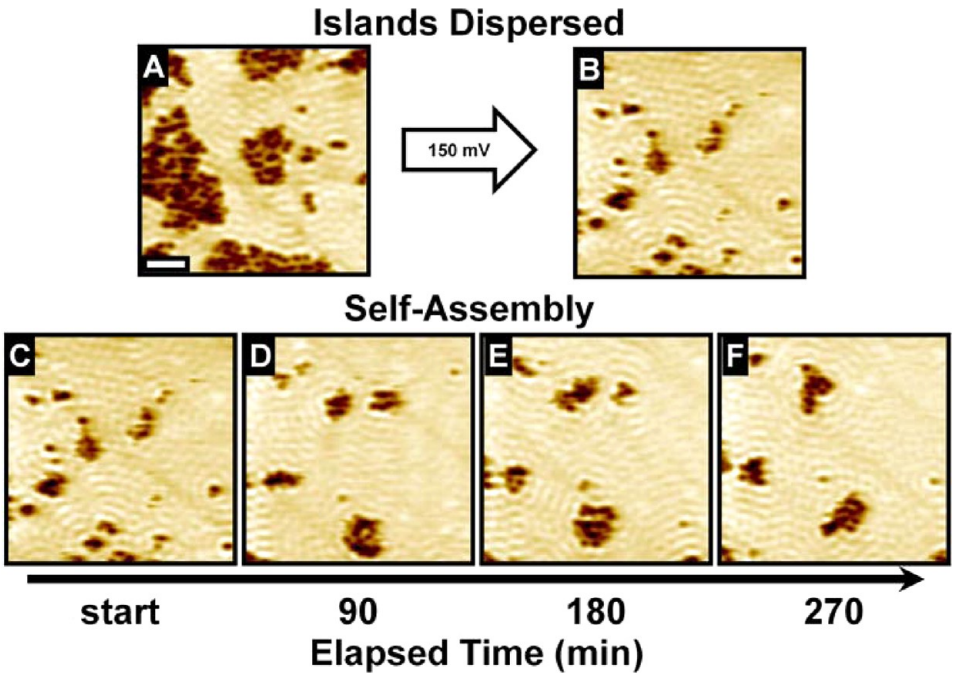

Figure 2. (A) STM image of H islands on Cu(111); the islands were dispersed by scanning at 150 mV, resulting in the system shown in panel B. (C−F) Time-lapse STM images showing the reassembly of H islands over 270 min at 5 K recorded using nonperturbative voltage and current. Scale bar = 5 nm.

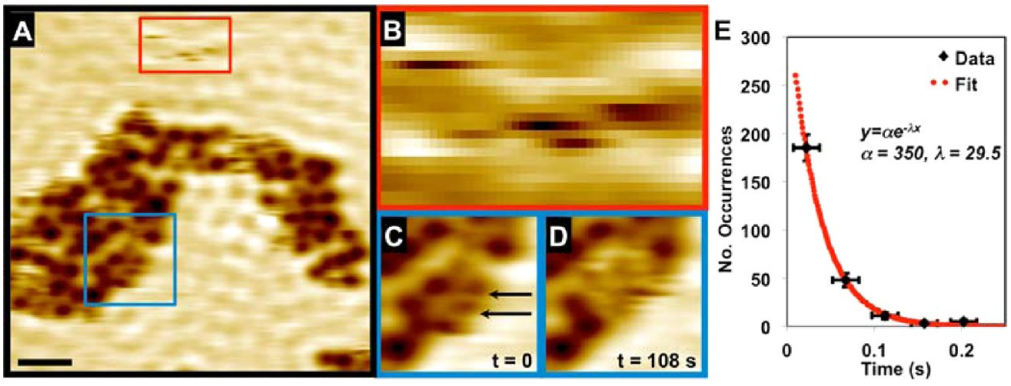

Figure 3. (A) STM image showing H clustering and islanding on the Cu surface. The red inset (B) shows the streaky appearance of a H monomer, which is diffusing much faster than STM imaging. The blue insets show two H monomers (indicated with black arrows) at the edge of an island both (C) before and (D) after diffusing away (time elapsed between panels C and D is 108 s). (E) Plot showing residence time data for H monomers; the rate of monomer diffusion can be estimated based on the exponential fit to the data. Scale bar = 3 nm.

as Supporting Information. In the case of H, we note that there is clear evidence for diffusion in the center and along the edges of the islands, and we observe that the island perimeters vary significantly over time. Conversely, there is very little diffusion of the D features over a similar 40 min interval. These data suggest that under identical scanning conditions and surface temperature, the diffusion rate of H is much faster than that of D.

The H islands were scattered by the STM tip when perturbative scanning conditions were employed. The effect is depicted in Figures 2A,B, where a gap voltage of 150 mV was deliberately used while scanning in order to disrupt the H islands and disperse them on the Cu terrace. Critically, upon continuing to scan under normal conditions (30 mV, 50 pA), reformation of the H island assemblies was observed as shown in the images in Figures 2C−F, which show the system at 90 min intervals. An STM movie of the H atom self-assembly is also available in the Supporting Information. These data clearly demonstrate that there is an attractive interaction between H species, and further characterization, described below, shows that the depressions seen in STM images are not in fact solely H monomers, but H monomers and clusters.

Figure 3 shows STM images of H on Cu(111) in which H atoms form small clusters that appear as depressions and congregate into islands. In this system (Figure 3A),

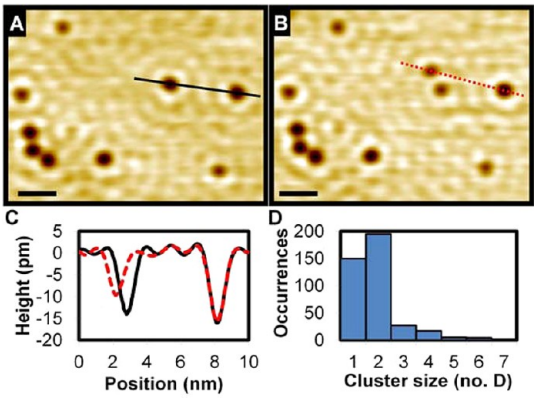

Figure 4. STM images showing D monomers and clusters on a Cu surface both (A) before and (B) after a dimer split into two monomers as the result of a low-voltage pulse with the STM tip. Scale bars = 3 nm. (C) Topographic profiles for lines shown in panel A (solid black) and B (dashed red) reveal that the monomer and dimer also differ in their apparent depth. (D) Histogram showing the relative abundance of D cluster types found on an unperturbed surface.

large islands of H clusters with well-defined boundaries are present. Occasionally, smaller features corresponding to H monomers appear at the island edges (Figure 3C), typically as a result of cluster splitting; however, these H monomers are transient and diffuse away by the next image (Figure 3D). Absolute cluster sizes were not easily determined in the H system due to rapid diffusion of H monomers during cluster splitting. However, the identities of D clusters were easier to investigate due to the slower motion in that system. Figure 4A shows D atoms on Cu(111) after the uptake of D_2 and cooling to 5 K demonstrating that the D atoms congregate into small clusters, but that the clusters do not assemble into islands. Figure 4 panels A and B show the D system before and after a dimer was split to monomers using a 100 mV pulse from the STM tip. From these images, it is clear that the D monomers and dimers appear differently on the Cu surface. Topographic line scans of a dimer pre- and post-splitting and that of an intact dimer (confirmed with voltage pulse after the image was recorded) are shown in Figure 4C. From this data we see that D monomers appear approximately two-thirds as deep as the dimers. The capability of using the STM tip to split each D feature into individual monomers with voltage pulses provided us with a reliable and straightforward way of determining D cluster size (i.e., number of atoms). Through interrogation of 400 D features, we reveal that the majority of these species are monomers (37%) and dimers (49%), with larger clusters being less common. A histogram showing the relative abundances of D cluster sizes is shown in Figure 4D.

Using DFT we have modeled the interactions between H atoms on Cu(111) by calculating the differential binding energy as a function of H coverage for $^1/_9$–$^7/_9$ monolayers (Figure 5). Consistent with previous reports, our calculations show that the most

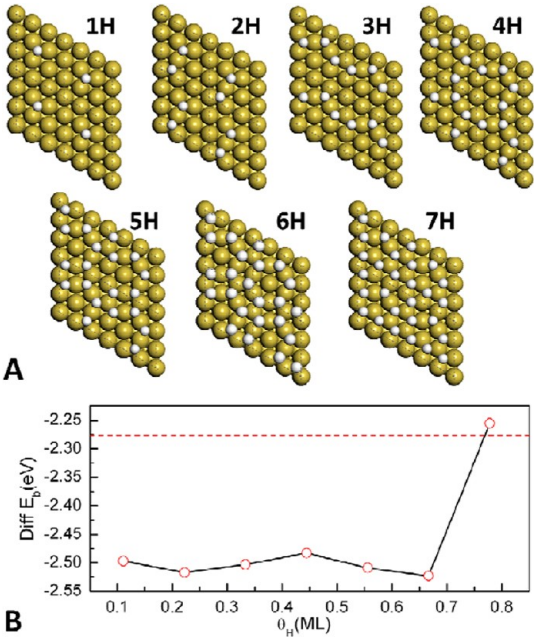

Figure 5. Schematics showing (A) the top view of the lowest energy configurations for H on Cu(111) for $^1/_9$ to $^7/_9$ monolayers and (B) the differential binding energy as a function of coverage (θ_H) in monolayers (ML) for H on Cu(111). The red dashed line indicates relative energy for H_2(g). Large yellow and small white spheres denote Cu and H atoms, respectively.

stable adsorption site for H is a 3-fold hollow.[34] In the most stable 2H configuration, the H atoms are arranged so that the second H atom is in the third nearest neighbor (3*NN*) position at a separation of 0.30 nm from the first one. This finding of an attractive 3*NN* interaction is consistent with previous calculations for H on Ni(111).[19,35,36] With the two H atoms arranged in this manner, one occupies an fcc 3-fold hollow site, while the other occupies an hcp 3-fold hollow site. If the second H atom is frozen in the second nearest neighbor (2*NN*) fcc position, the energy penalty is ~40 meV.[26] Also, according to our calculations, the fcc–hcp paired (2H) configuration is slightly more stable (by 20 meV) than the isolated atom (1H) and is the most stable low coverage (<0.5 ML) geometry examined. This result could explain why we observe both H and D in the form of clusters consisting predominantly of two atoms.

From high-resolution STM movies taken over several hours, the motion of H(D) monomers on Cu(111) was followed and the diffusion rate *k* was quantified. Figure 3 shows STM images in which H monomers are visible. These H monomers diffuse rapidly even at 5 K and move much faster than the time resolution of STM under normal scanning conditions, where each image requires 54 s to capture (imaging rate of 180 ms per line). Thus, H monomers appear as streaks of different thickness, as shown in Figures 3A,B. Due to the fast diffusion rate of isolated H atoms compared to the time scale of STM imaging, it was imperative to maximize

the instrument's temporal resolution. The time per line T_L is the product of T_R, the raster time (*i.e.*, time required for each pixel), and p, the number of pixels per line. Even with very fast scanning rates (15 ms/line), it was not possible to capture an image of complete H atoms before they moved on the surface. However, it was possible to determine the residence time of the atom before it moved by measuring the width of the feature in the slow scan direction before the next diffusional hop, that is, for how many line scans it was stationary. In this way the residence time of H atoms was measured, and the data was fit to an exponential plot with the formula $y = \alpha \exp^{-\lambda t}$, where λ gives the hop rate (Figure 3E). From 252 H hop events, we calculate k(H) $\approx$ 30 Hz. Due to the time-resolution of our instrument, in which the fastest scan speed to yield reliable data is 15 ms per line, this value suggests a lower limit for k(H). Unlike H monomers, D monomers diffuse slowly enough that these short-range diffusion events were easily captured, and k(D) was measured to be 3.2 $\pm$ 0.5 mHz, well below k(H). The rate of D dimer (2D) diffusion was measured to be 0.5 $\pm$ 0.4 mHz; these events included motion of the entire 2D species, as well as 2D splitting into monomers. The large error results from the low event frequency, which is an order of magnitude lower than for D monomers. It was previously established with energy electron loss spectroscopy (EELS)[37] and inelastic electron tunneling spectroscopy (STM-IETS)[21] that the H-Cu(D-Cu) vibrational stretch lies at 70(51) mV. The experiments here were performed at an imaging voltage of 30 mV, below the vibrational excitation energy in order to minimize the tip's influence on the diffusion rate. A similar set of nonperturbative tunneling conditions (40 mV, 100 pA) was used for the study of H(D) on Cu(001) by Ho and co-workers.[21] These facts, coupled with the slow motion observed in our D atom control experiments, allow us to conclude with reasonable certainty that the majority of the diffusion motion in the system arises from quantum tunneling of the adsorbates.

To elucidate the different behaviors of H and D diffusion at 5 K as observed in experiments, we calculated the diffusion rate of H(D) monomers and dimers on Cu(111). For H monomer diffusion on Cu(111), the calculated classical barrier height is 0.13 eV. At the experimental temperature of 5 K, the thermally activated diffusion rate calculated by the transition state theory, $k^{TST}(T) = \nu^{TST}(T) \exp(-E_a/(k_B T))$, is on the order of 10^{-102} Hz, which is infinitesimally small and can be ignored. After introducing the tunneling correction within the SC-TST approach, the calculated diffusion rate for the H monomer is 1.4×10^5 Hz, while the value for the D monomer is $\sim 10^3$ Hz. The calculated diffusion rate ratio of H and D at 5 K, $k^{TST}(H)/k^{TST}(D) = 145$, is in qualitative agreement with the experimental value of $\sim 10^4$. This explains why fast H diffusion was observed in low-temperature STM experiments at 5 K, while D diffusion is much slower, as shown in Figure 1.

To gain further insight into the slower D dimer (2D) diffusion compared with that of D monomer, we considered different diffusion pathways of a H(D) dimer. We first considered local motion in the form of dimer rotation around the central atom, in which the starting and ending 2H(2D) configurations were identical with one atom in an fcc site and the other in the *3NN,* hcp site. In the case where both atoms move simultaneously, the calculated E_a is 0.31 eV, more than twice what was calculated for monomer diffusion. In the case where the atoms move consecutively, the first motion results in a motion of a H(D) from the hcp site to the neighboring fcc site with $E_a \approx 0.16$ eV, and the second motion brings the other H(D) from the fcc site to the neighboring hcp site and returns the system to the lower energy arrangement with $E_a \approx 0.12$ eV. On the basis of these calculations, we propose that dimer diffusion follows the consecutive pathway, as the barrier for concerted motion is quite high. We also examined dimer separation (splitting) in which one atom moves from the 3*NN* hcp site to the fourth nearest neighbor (4*NN*) fcc site. Our calculations show that this separation results in a configuration that is less stable than the 3*NN* arrangement by $\sim$0.04 eV and has a barrier of $\sim$0.16 eV. For the first step motion of D dimer diffusion (*i.e.*, the step with a higher barrier of 0.16 eV) in the consecutive pathway, the calculated diffusion rate is 6 Hz within the SC-TST approach, which is 150 times slower than that of D monomer. This result qualitatively agrees with the experimental data and explains why the diffusion of D dimers is slower than that of D monomers.

CONCLUSIONS

The diffusion of H and D on Cu(111) was explored using STM at 5 K and periodic, self-consistent DFT calculations. We demonstrate that diffusion of both species at low temperature is enabled primarily by quantum tunneling. We also show the tunneling-enabled self-assembly of H(D) atoms, which can be explained in terms of local attractive pairwise interactions between atoms and leads to cluster formation. This stabilization also results in a slower rate of diffusion of clusters, as explicitly shown in the case of D. In the case of H, which diffuses fast due to higher tunneling probability, the $\sim$2H clusters aggregate into large islands of clusters that remain intact but constantly change in shape. D clusters, in contrast, have a much slower tunneling rate; hence, large scale self-assembly of D clusters was not observed over the time scale of our experiments. Given the difference in tunneling rates, we would presumably have to watch a D atom sample at 5 K for a period of >10000 h in order to directly observe the same large scale self-assembly of

islands of D clusters as was seen for H. What is perhaps most remarkable about our experiment is that unlike a thermally assisted self-assembly process in which higher order structures are "frozen out" as the temperature drops, quantum tunneling occurs down to 0 K. All the H atoms in the structures we observe are subject to constant quantum tunneling driven motion, but the self-assembled islands persist in a dynamic state and actually grow over time. To our knowledge, this study represents the first evidence for quantum-mechanical-tunneling enabled self-assembly of any species. Furthermore, the complex ordering behavior of H(D) atoms on a Cu(111) surface gives new physical insight into this important species on a catalytically relevant surface, revealing a very different picture of the geometry of H on Cu(111) as compared to all other metal surfaces studied to date.

EXPERIMENTAL AND COMPUTATIONAL METHODS

All STM experiments were performed in ultrahigh vacuum (UHV) using a low-temperature microscope manufactured by Omicron NanoTechnology. Images were acquired at 5 K and at a base pressure $<1 \times 10^{-11}$ mbar. The instrument incorporated a separate preparation chamber in which cleaning and Pd deposition were performed. The Cu(111) single crystal was prepared by cycles of Ar^+ sputtering and high temperature anneals, as previously described elsewhere,[38] and cleanliness was verified by STM imaging. Pd was deposited onto the clean Cu surface by physical vapor deposition using a Focus EFM 3 UHV electron beam evaporator. Hydrogen and deuterium gas were introduced to the clean sample at 5 K followed by a thermal anneal to 80 K. The sample was again cooled to 5 K for imaging. STM images were recorded at a sample bias range of 30−50 mV and a tunneling current range of 30−90 pA.

Periodic, self-consistent DFT calculations were performed using the VASP code[39,40] with the projector augmented wave (PAW) potentials.[41,42] The generalized gradient approximation (GGA-PW91)[43] was used to describe the exchange-correlation functional. The electron wave function was expanded using plane waves with an energy cutoff of 400 eV. The Cu(111) surface was modeled by a (3×3) surface unit cell in a slab with five layers of Cu atoms. A vacuum layer equivalent to six atomic layers along the *z*-direction was used between any two successive images of the slab. The calculated optimized lattice constant of $a_0 = 3.64$ Å was used for the Cu slab. The Brillouin zone of the Cu(111)-(3×3) surface was sampled by an $(8 \times 8 \times 1)$ k-point mesh based on the Monkhorst-Pack scheme.[44] Convergence with respect to the energy cutoff, k-point set, and number of metal layers in the slab was confirmed. The adsorbates and top three Cu layers of the slab were allowed to relax, while the bottom two layers were kept fixed. All atoms except for the fixed ones were fully relaxed until the Hellmann−Feynman forces were smaller than 0.01 eV/Å. The climbing image nudged elastic band method (CI-NEB)[45] was used to calculate the diffusion barriers. Vibrational frequencies were calculated by diagonalizing the Hessian matrix with the finite difference approach and a step-size of 0.015 Å.

The hopping rate of H(D) on Cu(111) was calculated using the semiclassically corrected transition state theory (SC-TST) following the Fermann and Auerbach approach.[46,47] Within the SC-TST framework, the hopping rate at temperature T is given by the equation $k^{\text{SC-TST}} = k^{\text{TST}}\Gamma(T)$, where k^{TST} is the transition state theory rate constant, and $\Gamma(T)$ is the tunneling correction factor. The transition state theory rate constant k^{TST} can be expressed as $k^{\text{TST}}(T) = \nu^{\text{TST}}(T)\exp(-E_a/k_BT)$, where the attempt frequency $\nu^{\text{TST}}(T)$ can be calculated by eq 1,

$$\nu^{\text{TST}}(T) = \frac{\prod_{i=1}^{3N} \nu_i \sinh(h\nu_i/2k_BT)/(h\nu_i/2k_BT)}{\prod_{j=1}^{3N-1} \nu_j^{\ddagger} \sinh(h\nu_j^{\ddagger}/2k_BT)/(h\nu_j^{\ddagger}/2k_BT)} \quad (1)$$

Here E_a is the classical barrier height, h is the Planck constant, k_B is the Boltzmann constant, and $\nu_i(\nu_j^{\ddagger})$ are the real vibrational frequencies of the initial (transition) state. The tunneling correction factor $\Gamma(T)$ is given by eq 2,

$$\Gamma(T) = \frac{\exp(E_a^{\text{ZPE}}/k_BT)}{1+\exp(2\pi E_a^{\text{ZPE}}/h|\nu_F^{\ddagger}|)} + \frac{1}{2}\int_{-\infty}^{\pi E_a^{\text{ZPE}}/h|\nu_F^{\ddagger}|} d\theta \exp\left(\frac{h|\nu_F^{\ddagger}|\theta}{\pi k_BT}\right) \text{sech}^2\theta \quad (2)$$

where E_a^{ZPE} is the zero-point-energy-corrected classical barrier height, and $\nu_F^{\ddagger}$ is the imaginary frequency of the transition state.

Conflict of Interest: The authors declare no competing financial interest.

Acknowledgment. We thank the U.S. Department of Energy (FG02-10ER16170) for financial support (M.M., C.M., G.K., E.S.). A.J. acknowledges the National Science Foundation for a Graduate Research Fellowship. E.L. thanks the Department of Education for a GAANN Fellowship. Work at UW-Madison has been supported by the DOE-BES, Office of Chemical Sciences. Computational work was performed in part using supercomputing resources from the following institutions: EMSL, a National scientific user facility at Pacific Northwest National Laboratory (PNNL); the Center for Nanoscale Materials at Argonne National Laboratory (ANL); the National Center for Computational Sciences at Oak Ridge National Laboratory (ORNL); and the National Energy Research Scientific Computing Center (NERSC). EMSL is sponsored by the Department of Energy's Office of Biological and Environmental Research located at PNNL. CNM, NCCS, and ORNL are supported by the U.S. Department of Energy, Office of Science, under Contracts DE-AC02-06CH11357, DEAC05-00OR22725, and DE-AC02-05CH11231, respectively.

Supporting Information Available: STM movies showing hydrogen and deuterium diffusion and hydrogen self-assembly at 5 K. This material is available free of charge *via* the Internet at http://pubs.acs.org.

REFERENCES AND NOTES

1. Bartels, L. Tailoring Molecular Layers at Metal Surfaces. *Nat. Chem.* **2010**, *2*, 87–95.
2. Barth, J. V. Molecular Architectonic on Metal Surfaces. *Annu. Rev. Phys. Chem.* **2007**, *58*, 375–407.
3. Sykes, E. C. H.; Han, P.; Kandel, S. A.; Kelly, K. F.; McCarty, G. S.; Weiss, P. S. Substrate-Mediated Interactions and Intermolecular Forces between Molecules Adsorbed on Surfaces. *Acc. Chem. Res.* **2003**, *36*, 945–953.
4. Han, P.; Weiss, P. S. Electronic Substrate-Mediated Interactions. *Surf. Sci. Rep.* **2012**, *67*, 19–81.
5. Love, J. C.; Estroff, L. A.; Kriebel, J. K.; Nuzzo, R. G.; Whitesides, G. M. Self-Assembled Monolayers of Thiolates on Metals as a Form of Nanotechnology. *Chem. Rev.* **2005**, *105*, 1103–1169.
6. Smith, R. K.; Lewis, P. A.; Weiss, P. S. Patterning Self-Assembled Monolayers. *Prog. Surf. Sci.* **2004**, *75*, 1–68.
7. Nuzzo, R. G.; Allara, D. L. Adsorption of Bifunctional Organic Disulfides on Gold Surfaces. *J. Am. Chem. Soc.* **1983**, *105*, 4481–4483.
8. Poirier, G. E.; Pylant, E. D. The Self-Assembly Mechanism of Alkanethiols on Au(111). *Science* **1996**, *272*, 1145–1148.
9. Bucher, J.-P.; Santesson, L.; Kern, K. Thermal Healing of Self-Assembled Organic Monolayers: Hexane- and Octadecanethiol on Au(111) and Ag(111). *Langmuir* **1994**, *10*, 979–983.

10. Delamarche, E.; Michel, B.; Kang, H.; Gerber, C. Thermal Stability of Self-Assembled Monolayers. *Langmuir* **1994**, *10*, 4103–4108.
11. Zambelli, T.; Barth, J. V.; Wintterlin, J.; Ertl, G. Complex Pathways in Dissociative Adsorption of Oxygen on Platinum. *Nature* **1997**, *390*, 495–497.
12. Lin, T.-S.; Gamer, R. Diffusion of 1H and 2H on the Ni(111) and (100) Planes. *Surf. Sci.* **1991**, *255*, 41–60.
13. DiFoggio, R.; Gomer, R. Diffusion of Hydrogen and Deuterium on the (110) Plane of Tungsten. *Phys. Rev. B* **1982**, *25*, 3490–3511.
14. Dharmadhikari, C.; Gomer, R. Diffusion of Hydrogen and Deuterium on the (111) Plane of Tungsten. *Surf. Sci.* **1984**, *143*, 223–242.
15. Wang, S. C.; Gomer, R. Diffusion of Hydrogen, Deuterium, and Tritium on the (110) Plane of Tungsten. *J. Chem. Phys.* **1985**, *83*, 4193–4209.
16. Daniels, E. A.; Lin, J. C.; Gomer, R. Diffusion Anisotropy of Hydrogen and Deuterium on the Tungsten (211) Plane. *Surf. Sci.* **1988**, *204*, 129–146.
17. Lee, A.; Zhu, X. D.; Deng, L.; Linke, U. Observation of a Transition from Over-Barrier Hopping to Activated Tunneling Diffusion: H and D on Ni(100). *Phys. Rev. B* **1992**, *46*, 472–476.
18. Lee, A.; Zhu, X. D.; Wong, A.; Deng, L.; Linke, U. Observation of Diffusion of H and D on Ni(111) from Over-Barrier Hopping to Nonactivated Tunneling. *Phys. Rev. B* **1993**, *48*, 256–259.
19. Wong, A.; Lee, A.; Zhu, X. D. Coverage Dependence of Quantum Tunneling Diffusion of Hydrogen and Deuterium on Ni(111). *Phys. Rev. B* **1995**, *51*, 4418–4425.
20. Wang, X.; Fei, Y. Y.; Zhu, X. D. Classical and Quantum Diffusion of Hydrogen Atoms on Cu(111). *Chem. Phys. Lett.* **2009**, *481*, 58–61.
21. Lauhon, L. J.; Ho, W. Direct Observation of the Quantum Tunneling of Single Hydrogen Atoms with a Scanning Tunneling Microscope. *Phys. Rev. Lett.* **2000**, *85*, 4566–4569.
22. Kua, J.; Lauhon, L. J.; Ho, W.; Goddard, W. A. Direct Comparisons of Rates for Low Temperature Diffusion of Hydrogen and Deuterium on Cu(001) from Quantum Mechanical Calculations and Scanning Tunneling Microscopy Experiments. *J. Chem. Phys.* **2001**, *115*, 5620–5624.
23. Heinrich, A. J.; Lutz, C. P.; Gupta, J. A.; Eigler, D. M. Molecule Cascades. *Science* **2002**, *298*, 1381–1387.
24. Pawin, G.; Wong, K. L.; Kwon, K.-Y.; Frisbee, R. J.; Rahman, T. S.; Bartels, L. Surface Diffusive Motion in a Periodic and Asymmetric Potential. *J. Am. Chem. Soc.* **2008**, *130*, 15244–15245.
25. Stroscio, J. A.; Tavazza, F.; Crain, J. N.; Celotta, R. J.; Chaka, A. M. Electronically Induced Atom Motion Engineered $CoCu_n$ Nanostructures. *Science* **2006**, *313*, 948–951.
26. Repp, J.; Meyer, G.; Rieder, K.-H.; Hyldgaard, P. Site Determination and Thermally Assisted Tunneling in Homogenous Nucleation. *Phys. Rev. Lett.* **2003**, *91*, 2061021–2061024.
27. Mattsson, T.; Wahnström, G. Isotope Effect in Hydrogen Surface Diffusion. *Phys. Rev. B* **1997**, *56*, 14944–14947.
28. Mattsson, T.; Engberg, U.; Wahnström, G. H Diffusion on Ni(100): A Quantum Monte Carlo Simulation. *Phys. Rev. Lett.* **1993**, *71*, 2615–2618.
29. Chen, L.; Ying, S. Theory of Surface Diffusion: Crossover from Classical to Quantum Regime. *Phys. Rev. Lett.* **1994**, *73*, 700–703.
30. Kammler, T.; Küppers, J. Interaction of H Atoms with Cu(111) Surfaces: Adsorption, Absorption, and Abstraction. *J. Chem. Phys.* **1999**, *111*, 8115–8123.
31. Kyriakou, G.; Boucher, M. B.; Jewell, A. D.; Lewis, E. A.; Lawton, T. J.; Baber, A. E.; Tierney, H. L.; Flytzani-Stephanopoulos, M.; Sykes, E. C. H. Isolated Metal Atom Geometries as a Strategy for Selective Heterogeneous Hydrogenations. *Science* **2012**, *335*, 1209–1212.
32. Tierney, H. L.; Baber, A. E.; Kitchin, J. R.; Sykes, E. C. H. Hydrogen Dissociation and Spillover on Individual Isolated Palladium Atoms. *Phys. Rev. Lett.* **2009**, *103*, 2461021–2461024.
33. Mitsui, T.; Rose, M. K.; Fomin, E.; Ogletree, D. F.; Salmeron, M. Dissociative Hydrogen Adsorption on Palladium Requires Aggregates of Three or More Vacancies. *Nature* **2003**, *422*, 705–707.
34. Luo, M. F.; Hu, G. R.; Lee, M. H. Surface Structures of Atomic Hydrogen Adsorbed on Cu(111) Surface Studied by Density-Functional-Theory Calculations. *Surf. Sci.* **2007**, *601*, 1461–1466.
35. Domany, E.; Schick, M.; Walker, J. S. Proposed Structure of Hydrogen on Ni(111). *Solid State Commun.* **1979**, *30*, 331–332.
36. Walker, J.; Schick, M. Order–Disorder Transitions to 2×2 Structures. *Phys. Rev. B* **1979**, *20*, 2088–2096.
37. Chorkendorff, I.; Rasmussen, P. B. Reconstruction of Cu-(100) by Adsorption of Atomic Hydrogen. *Surf. Sci.* **1991**, *248*, 35–44.
38. Jewell, A.; Tierney, H. L.; Baber, A. E.; Iski, E. V.; Laha, M. M.; Sykes, E. C. H. Time-Resolved Studies of Individual Molecular Rotors. *J. Phys.: Condensed Matter* **2010**, *22*, 2640061–26400611.
39. Kresse, G.; Furthmüller, J. Efficiency of *ab-Initio* Total Energy Calculations for Metals and Semiconductors Using a Plane-Wave Basis Set. *Comput. Mater. Sci.* **1996**, *6*, 15–50.
40. Kresse, G.; Furthmüller, J. Efficient Iterative Schemes for *ab Initio* Total-Energy Calculations Using a Plane-Wave Basis Set. *Phys. Rev. B* **1996**, *54*, 11169–11186.
41. Kresse, G.; Joubert, D. From Ultrasoft Pseudopotentials to the Projector Augmented-Wave Method. *Phys. Rev. B* **1999**, *59*, 1758–1775.
42. Blöchl, P. E. Projector Augmented-Wave Method. *Phys. Rev. B* **1994**, *50*, 17953–17979.
43. Perdew, J. P.; Wang, Y. Accurate and Simple Analytic Representation of the Electron-Gas Correlation Energy. *Phys. Rev. B* **1992**, *45*, 13244–13249.
44. Monkhorst, H. J.; Pack, J. D. Special Points for Brillouin-Zone Integrations. *Phys. Rev. B* **1976**, *13*, 5188–5192.
45. Henkelman, G.; Uberuaga, B. P.; Jónsson, H. A Climbing Image Nudged Elastic Band Method for Finding Saddle Points and Minimum Energy Paths. *J. Chem. Phys.* **2000**, *113*, 9901–9904.
46. Fermann, J. T.; Auerbach, S. Modeling Proton Mobility in Acidic Zeolite Clusters: II. Room Temperature Tunneling Effects from Semiclassical Rate Theory. *J. Chem. Phys.* **2000**, *112*, 6787–6794.
47. Bhatia, B.; Sholl, D. Quantitative Assessment of Hydrogen Diffusion by Activated Hopping and Quantum Tunneling in Ordered Intermetallics. *Phys. Rev. B* **2005**, *72*, 2243021–2243028.